



HAL
open science

Role of the N-terminal region for the conformational stability of esterase 2 from *Alicyclobacillus acidocaldarius*

Fabrizia Foglia, Luigi Mandrich, Margherita Pezzullo, Giuseppe Graziano, Guido Barone, Mosè Rossi, Giuseppe Manco, Pompea Del Vecchio

► To cite this version:

Fabrizia Foglia, Luigi Mandrich, Margherita Pezzullo, Giuseppe Graziano, Guido Barone, et al.. Role of the N-terminal region for the conformational stability of esterase 2 from *Alicyclobacillus acidocaldarius*. *Biophysical Chemistry*, 2007, 127 (1-2), pp.113. 10.1016/j.bpc.2007.01.004 . hal-00501634

HAL Id: hal-00501634

<https://hal.science/hal-00501634>

Submitted on 12 Jul 2010

HAL is a multi-disciplinary open access archive for the deposit and dissemination of scientific research documents, whether they are published or not. The documents may come from teaching and research institutions in France or abroad, or from public or private research centers.

L'archive ouverte pluridisciplinaire **HAL**, est destinée au dépôt et à la diffusion de documents scientifiques de niveau recherche, publiés ou non, émanant des établissements d'enseignement et de recherche français ou étrangers, des laboratoires publics ou privés.

Accepted Manuscript

Role of the N-terminal region for the conformational stability of esterase 2 from *Alicyclobacillus acidocaldarius*

Fabrizia Foglia, Luigi Mandrich, Margherita Pezzullo, Giuseppe Graziano, Guido Barone, Mosè Rossi, Giuseppe Manco, Pompea Del Vecchio

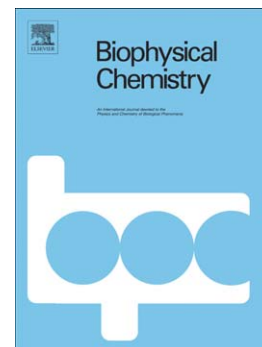
PII: S0301-4622(07)00010-5
DOI: doi: [10.1016/j.bpc.2007.01.004](https://doi.org/10.1016/j.bpc.2007.01.004)
Reference: BIOCHE 4922

To appear in: *Biophysical Chemistry*

Received date: 24 November 2006
Revised date: 10 January 2007
Accepted date: 10 January 2007

Please cite this article as: Fabrizio Foglia, Luigi Mandrich, Margherita Pezzullo, Giuseppe Graziano, Guido Barone, Mosè Rossi, Giuseppe Manco, Pompea Del Vecchio, Role of the N-terminal region for the conformational stability of esterase 2 from *Alicyclobacillus acidocaldarius*, *Biophysical Chemistry* (2007), doi: [10.1016/j.bpc.2007.01.004](https://doi.org/10.1016/j.bpc.2007.01.004)

This is a PDF file of an unedited manuscript that has been accepted for publication. As a service to our customers we are providing this early version of the manuscript. The manuscript will undergo copyediting, typesetting, and review of the resulting proof before it is published in its final form. Please note that during the production process errors may be discovered which could affect the content, and all legal disclaimers that apply to the journal pertain.



**Role of the N-terminal region for the conformational stability of esterase 2 from
*Alicyclobacillus acidocaldarius***

Fabrizia Foglia^{a*}, Luigi Mandrich^{b*}, Margherita Pezzullo^b, Giuseppe Graziano^c, Guido Barone^a, Mosè Rossi^b, Giuseppe Manco^b and Pompea Del Vecchio^{a, d}

^aDipartimento di Chimica, Università di Napoli Federico II, Via Cintia, 80126 Napoli, Italy

^bIstituto di Biochimica delle Proteine, CNR, Via P. Castellino 111, 80131 Napoli, Italy

^cDipartimento di Scienze Biologiche ed Ambientali, Università del Sannio, Via Port'Arso 11,
82100 Benevento, Italy

* These authors contributed equally to this paper

^dTo whom correspondence should be addressed

phone: +39/081/674255; Fax: +39/081/674257

E-mail: pompea.delvecchio@unina.it

Abstract

In order to clarify the role played by the N-terminal region for the conformational stability of the thermophilic esterase 2 (EST2) from *Alicyclobacillus acidocaldarius*, two mutant forms have been investigated: a variant obtained by deleting the first 35 residues at the N-terminus (EST2-36del), and a variant obtained by mutating Lys102 to Gln (K102Q) to perturb the N-terminus by destroying the salt bridge E43-K102. The temperature- and denaturant-induced unfolding of EST2 and the two mutant forms have been studied by means of circular dichroism (CD), differential scanning calorimetry (DSC) and fluorescence measurements. In line with its thermophilic origin, the denaturation temperature of EST2 is high: $T_d = 91\text{ }^\circ\text{C}$ and $86\text{ }^\circ\text{C}$ if detected by recording the CD signal at 222 nm and 290 nm, respectively. This difference suggests that the thermal denaturation process, even though reversible, is more complex than a two-state $N \rightleftharpoons D$ transition. The non-two-state behaviour is more pronounced in the case of the two mutant forms. The complex DSC profiles of EST2 and both mutant forms have been analysed by means of a deconvolution procedure. The thermodynamic parameters characterizing the two transitions obtained in the case of EST2 are: $T_{d,1} = 81\text{ }^\circ\text{C}$, $\Delta_d H_1 = 440\text{ kJ mol}^{-1}$, $\Delta_d C_{p,1} = 7\text{ kJ K}^{-1}\text{mol}^{-1}$, $T_{d,2} = 86\text{ }^\circ\text{C}$, $\Delta_d H_2 = 710\text{ kJ mol}^{-1}$, and $\Delta_d C_{p,2} = 9\text{ kJ K}^{-1}\text{mol}^{-1}$. The first transition occurs at lower temperatures in the two mutant forms, whereas the second transition is always centred at $86\text{ }^\circ\text{C}$. The results indicate that EST2 possesses two structural domains whose coupling is tight in the wild-type protein, but markedly weakens in the two mutant forms as a consequence of the perturbations in the N-terminal region.

Keywords: thermophilic esterase, conformational stability, independent or sequential two-state transitions, coupled domains.

Abbreviations. EST2, esterase from *Alicyclobacillus acidocaldarius*; HSL, hormone sensitive lipase family; GuHCl, guanidine hydrochloride; pNP, p-nitrophenyl; CD, circular dichroism; DSC, differential scanning calorimetry; HPLC, high performance liquid chromatography; SDS-PAGE, sodium dodecyl sulfate-polyacrylamide gel electrophoresis.

1. Introduction

In recent years a thermophilic esterase of 310 residues, called EST2 [1,2], belonging to the hormone sensitive lipase, HSL, family [3], has been isolated from *Alicyclobacillus acidocaldarius*, and subsequently cloned and overexpressed in *E.coli*. Its catalytic triad has been identified (i.e., Ser155, Asp252 and His282) [4]; the enzymatic activity [2,5], and the conformational stability against temperature and chemical denaturants [6-8] have been investigated in detail. The 3D structure of EST2 has been solved by X-ray diffraction to 2.6 Å resolution, PDB code 1EVQ [9,10], and is shown in Figure 1a. The protein possesses the classical α/β hydrolase fold with a central β -sheet, consisting of eight strands highly twisted, surrounded by nine α -helices; a topology model of the structure is shown in Figure 1b. A careful examination of the structure led to the identification of a “cap” domain, constituted by helices α_1 , α_2 , α_6 and α_7 , partially covering the entrance of the active site cleft. It has been argued that the “cap” domain could play a role in modulating the catalytic activity of EST2 [11], rendering it very low towards triacylglycerols, the natural substrates of lipases. On this basis a variant of EST2 has been engineered by deleting the first 35 residues in the sequence, called EST2-36del, in order to verify its activity against triacylglycerols [11]. The matter, however, proved to be more complex than expected because EST2-36del showed a lower activity with respect to the parent enzyme towards all tested substrates; in particular it showed a markedly reduced activity towards pNP esters [11].

On the other hand, this deleted variant showed an optimal temperature against pNP-hexanoate of 50 °C, whereas EST2 has an optimal temperature of 70 °C. In addition, the residual activity after incubation at 70 °C for two hours is 70% of its initial value for EST2-36del and 100% for wild-type EST2. These kinetic data indicated that the first 35 residues of the protein play a role in the conformational stability of EST2, a role that merits further investigation by means of thermodynamic approaches. Moreover, a second variant has been engineered by mutating Lys102 to Gln in order to destroy a strong salt-bridge existing between the side chains of Glu43 and Lys102 [9]. This salt-bridge connects the core of the protein structure to the N-terminal region (i.e., the same region deleted in EST2-36del), as can be appreciated by looking at Figures 1a and 1b. In fact, both Ser35 and Glu43 occur in a long loop, spanning residues 33-46, linking helix α_2 (residues 27-32) to strand β_1 (residues 47-55).

Circular dichroism, CD, and differential scanning calorimetry, DSC, measurements have been performed to investigate in detail the thermal unfolding of EST2, K102Q and EST2-36del. Experimental data indicate that the temperature-induced unfolding of all the three proteins is a reversible process that cannot be represented as a two-state $N \rightleftharpoons D$ transition. Deconvolution of DSC curves has allowed the determination of the thermodynamic parameter values characterizing the two component transitions. A reliable identification of the EST2 domains responsible of such behaviour is proposed, taking into account the available structural information.

2. Experimental

2.1. Protein preparation. EST2 and EST2-36del were overexpressed in *E.coli* and purified according to the procedure previously described [2,11]. Mutant K102Q was produced by site directed mutagenesis. Details on protein overexpression, purification and kinetic characterization will be published elsewhere (M. Pezzullo et al. in preparation). SDS-PAGE and reversed-phase HPLC were used to check the purity of homogeneous preparations. An Amicon ultrafiltration apparatus was used to concentrate protein samples after exhaustive dialysis. Protein concentration was measured spectrophotometrically using $\epsilon(280 \text{ nm}) = 43360 \text{ M}^{-1}\text{cm}^{-1}$ for EST2 and K102Q, and $42080 \text{ M}^{-1}\text{cm}^{-1}$ for EST2-36del, calculated from Tyr and Trp residues absorption [12]. A buffer solution, consisting of 20 mM sodium phosphate at pH 7.5, was used in all denaturation experiments. Chemical denaturants, urea and GuHCl, were from Sigma (Sigma Chemicals, St.Louis, Missouri). Urea was used after recrystallization from ethanol/water (1:1) mixtures; urea solutions were prepared immediately before use and the concentration determined by refractive index measurements [13]. A commercial 8 M solution was used for GuHCl. Protein solutions were exhaustively dialyzed by using Spectra Por MW 15000-17000 membranes against buffer solution at 4 °C. The water used for buffer and sample solutions was deionized and filtered through a Millipore Elix3 reagent grade system. The pH was measured at 25 °C with a Radiometer pHmeter model PHM93. Stock solutions of urea and GuHCl, in different amounts, were mixed with protein solution to give constant, fixed final protein concentration. The final concentrations ranged from 0 to 9 M for urea, and from 0 to 6 M for GuHCl. Since high urea or GuHCl concentrations change the pH, the final pH for each sample was corrected by addition of concentrated solutions of HCl or NaOH.

Each sample was mixed by vortexing and was incubated overnight at 4 °C. Longer incubation times produce identical spectroscopic signals.

2.2. *Circular dichroism.* CD spectra were recorded with a Jasco J-715 spectropolarimeter equipped with a Peltier type temperature control system (Model PTC-348WI). The instrument has been calibrated with an aqueous solution of d-10-(+)-camphorsulfonic acid at 290 nm [14]. Molar ellipticity per mean residue, $[\theta]$ in $\text{deg cm}^2 \text{ dmol}^{-1}$, was calculated from the equation: $[\theta] = [\theta]_{\text{obs}} \cdot \text{mrw} / 10 \cdot l \cdot C$, where $[\theta]_{\text{obs}}$ is the ellipticity measured in degrees, mrw is the mean residue molecular weight, 113 Da, C is the protein concentration in g mL^{-1} and l is the optical path length of the cell in cm. Cuvettes of 0.2 and 1 cm path length and protein concentrations of about 0.1 and 1 mg mL^{-1} were used in the far-UV and near-UV region, respectively. CD spectra recorded at 20 °C with a time constant of 4 s, a 2 nm band width and a scan rate of 5 nm min^{-1} were signal-averaged over at least five scans, and baseline was corrected by subtracting a buffer spectrum. Analysis of the spectra has been done using the Selcon method [15], as implemented in Dichroweb [16]. Thermal unfolding curves were recorded in the temperature mode at both 222 nm and 290 nm, using a scanning rate of 1.0 K min^{-1} .

2.3. *Fluorescence measurements.* Steady-state fluorescence measurements were performed with a JASCO FP-750 spectrofluorimeter equipped with thermostated cell holders and temperature was kept constant by a circulating water bath. The protein concentration ranges from 0.01 to 0.02 mg mL^{-1} . The excitation wavelength was set at 280 nm in order to include the contribution of Tyr residues to the overall fluorescence emission [17]. The experiments were performed at 20 °C by using a 1 cm sealed cell and a 5 nm emission slit width, and corrected for background signal. Both the change in fluorescence intensity and the shift in fluorescence maximum wavelength were recorded to monitor the unfolding transition.

2.4. *Differential scanning calorimetry.* DSC measurements were carried out on a Setaram Micro-DSC III instrument, interfaced with a data translation A/D board for automatic data acquisition. Data analysis was performed with in-house programs [18]. A scan rate of 1.0 K min^{-1} was chosen for all experiments, and protein concentration ranged from 1 to 2 mg mL^{-1} . The raw data were converted to an apparent heat capacity by correcting for the instrument calibration curve and the buffer-buffer scanning curve and by dividing each data point by the scan rate and the

protein molar concentration in the sample cell. Finally, the excess heat capacity function, $\langle \Delta C_p \rangle$, was obtained by subtraction of the baseline, given by linear extrapolation of the heat capacity of the native state [19]. The van't Hoff enthalpy is calculated by the commonly used formula [20]:

$$\Delta_d H(vH) = 4R T_d^2 \langle \Delta C_p(T_d) \rangle / \Delta_d H \quad (1)$$

where T_d is the denaturation temperature corresponding to the maximum of DSC peak, $\langle \Delta C_p(T_d) \rangle$ is the height of the excess heat capacity at T_d , $\Delta_d H$ is the total denaturation enthalpy change calculated by direct integration of the area of the DSC peak, and R is the gas constant. The finding that the calorimetric to van't Hoff enthalpy ratio is close to one is a necessary condition to state that the denaturation is a two-state transition [20,21].

2.5. Deconvolution of DSC curves. We consider the presence of two conformational transitions that may be independent of each other or sequential [22]. K_1 is the equilibrium constant of the first conformational transition, and is temperature dependent according to:

$$K_1 = \exp -\{(\Delta_d H_1/R) [(1/T) - (1/T_{d,1})] + (\Delta_d C_{p,1}/R)[1 - (T_{d,1}/T) - \ln(T/T_{d,1})]\} \quad (2)$$

where $T_{d,1}$ is the denaturation temperature at which $K_1 = 1$, $\Delta_d H_1$ is the enthalpy change associated with the first transition and $\Delta_d C_{p,1}$ the corresponding heat capacity change. Similarly, K_2 is the equilibrium constant of the second conformational transition, and is temperature dependent according to:

$$K_2 = \exp -\{(\Delta_d H_2/R) [(1/T) - (1/T_{d,2})] + (\Delta_d C_{p,2}/R)[1 - (T_{d,2}/T) - \ln(T/T_{d,2})]\} \quad (3)$$

where $T_{d,2}$ is the denaturation temperature at which $K_2 = 1$, $\Delta_d H_2$ is the enthalpy change associated with the second transition and $\Delta_d C_{p,2}$ the corresponding heat capacity change. Equations (2) and (3) are exact in the assumption that the heat capacity changes are temperature independent. By assuming the native state as reference, the macroscopic canonical partition function for the independent model is:

$$Q_{\text{IND}}(T) = (1 + K_1) \cdot (1 + K_2) \quad (4)$$

and for the sequential model is:

$$Q_{\text{SEQ}}(T) = 1 + K_1 + K_1 K_2 \quad (5)$$

The corresponding excess enthalpy functions with respect to the native state, obtained by means of a general statistical mechanical relationship [19,22,23], are:

$$\begin{aligned} \langle \Delta H(T) \rangle_{\text{IND}} = & [\Delta_d H_1 + \Delta_d C_{p,1}(T - T_{d,1})] \cdot [K_1 / (1 + K_1)] + [\Delta_d H_2 + \\ & + \Delta_d C_{p,2}(T - T_{d,2})] \cdot [K_2 / (1 + K_2)] \end{aligned} \quad (6)$$

$$\begin{aligned} \langle \Delta H(T) \rangle_{\text{SEQ}} = & [\Delta_d H_1 + \Delta_d C_{p,1}(T - T_{d,1})] \cdot (K_1 / Q_{\text{SEQ}}) + [\Delta_d H_1 + \Delta_d C_{p,1}(T - T_{d,1}) + \\ & + \Delta_d H_2 + \Delta_d C_{p,2}(T - T_{d,2})] \cdot (K_1 K_2 / Q_{\text{SEQ}}) \end{aligned} \quad (7)$$

In general, the excess heat capacity function, which is the physical observable of DSC measurements, is simply given by the temperature derivative of $\langle \Delta H(T) \rangle$ [19]. DSC curves can be directly simulated by using as input parameters the values of $T_{d,1}$, $\Delta_d H_1$, $\Delta_d C_{p,1}$, $T_{d,2}$, $\Delta_d H_2$ and $\Delta_d C_{p,2}$: these are the parameters to be determined by the deconvolution analysis of experimental DSC curves. Deconvolution of experimental peaks is performed by means of a nonlinear regression, using the Levenberg-Marquardt algorithm, as implemented in the Optimization Toolbox of MATLAB, for both the independent and the sequential models.

3. Results

Far-UV CD spectra of EST2, K102Q and EST2-36del, recorded at 20 °C and 108 °C, pH 7.5, 20 mM phosphate buffer, are shown in Figure 2a. Room temperature spectra indicate that the three proteins possess the same content of secondary structure elements, 40% α -helix and 20% β -sheet, in line with the X-ray structure of EST2 [6,9]. Near-UV CD spectra of EST2, K102Q and EST2-36del, recorded at 20 °C and 108 °C, pH 7.5, 20 mM phosphate buffer, are shown in Figure

2b. The environment of aromatic side chains is closely similar in the first two proteins, instead the absence of the positive CD band centred at 270 nm in the spectrum of EST2-36del can be attributed to the loss of Tyr22. Spectra recorded at 108 °C indicate that, at high temperature, all proteins show a residual secondary structure, but have no detectable tertiary structure.

Thermal unfolding curves have been obtained for the three proteins at pH 7.5, 20 mM phosphate buffer, in the far-UV and near-UV regions, by recording the molar ellipticity at 222 nm and 290 nm, using a scanning rate of 1.0 K min⁻¹. They are shown in Figures 3-5. Thermal unfolding proves to be a reversible process for the three proteins, as demonstrated by the reheating criterion (see Figure 6). Visual inspection of such curves unequivocally indicates that the thermal unfolding of all the three proteins is not a two-state N \rightleftharpoons D transition. This is especially evident in the case of K102Q and EST2-36del because thermal unfolding curves recorded at 290 nm present two inflection points indicative of two temperature-induced transitions. The shape of the curves recorded at 222 nm is less complex, and could be suggestive of a cooperative, all-or-none, transition. Indeed, in previous investigations, on the basis of thermal unfolding curves recorded at 222 nm and 270 nm, we concluded that the temperature-induced denaturation of EST2 is a two-state N \rightleftharpoons D transition [6]. According to the present data, especially those recorded at 290 nm, that conclusion has to be considered not correct. It appears that, in the case of EST2, the CD signal at 222 nm, representative of the protein secondary structure, is not a good probe to follow the thermal unfolding. In fact, for EST2, the inflection point occurs at 91 °C by recording the molar ellipticity at 222 nm, and at 86 °C by recording the molar ellipticity at 290 nm (see the values reported in Table 1); apparently, the tertiary structure unfolds at a lower temperature than the secondary one.

To reach a better understanding of the temperature-induced unfolding and to obtain precise thermodynamic data on the two component transitions, DSC measurements have been performed at pH 7.5, 20 mM phosphate buffer, using a scanning rate of 1.0 K min⁻¹. The DSC reheating criterion confirms that the thermal unfolding is a reversible process for all the three proteins (not shown). Experimental DSC curves are shown in Figure 7 and raw data are collected in Table 1. Inspection of DSC traces indicate that: (a) the process is not a two-state N \rightleftharpoons D transition for all the three proteins; (b) the temperature of the larger maximum corresponds to the inflection point at higher temperature of the transition curve recorded at 290 nm (see Table 1); (c) the calorimetric enthalpy change,

obtained by direct integration of the area under the DSC curves, is significantly larger than the van't Hoff enthalpy values calculated by analysing both CD and DSC curves in the assumption that the process can be represented as a two-state $N \rightleftharpoons D$ transition (see the numbers listed in Table 1). A more careful analysis is needed.

Deconvolution of experimental DSC curves has been performed by means of two procedures [22]: (a) assuming that the process can be represented as the sum of two independent two-state transitions (i.e., the so-called independent model); (b) assuming that the process can be represented by two sequential two-state transitions (i.e., the so-called sequential model). The curves calculated by means of the independent model are superimposed on the experimental ones in Figure 7. The numerical values of the thermodynamic parameters for the component transitions are listed in Table 2, and prove to be similar for both approaches. At first sight this finding may appear strange, but it is directly related to the fact that the two transitions differ significantly in the T_d and $\Delta_d H$ values, as underscored long time ago by Gill, Wyman and co-workers [24]. According to the independent model, it results that: (a) the first transition, domain-1, is characterized by $T_{d,1} = 81$ °C for EST2, 76 °C for K102Q and 62 °C for EST2-36del; correspondingly the $\Delta_d H_1$ value decreases from 440 kJ mol⁻¹ for the first two proteins to 300 kJ mol⁻¹ for EST2-36del: such a decrease in the enthalpy change can largely be explained by considering that $\Delta_d C_{p,1} = 7$ kJ K⁻¹mol⁻¹ for all the three proteins; (b) the second transition, domain-2, is characterized by $T_{d,2} = 86$ °C for all the three proteins, the $\Delta_d H_2$ value gradually decreases from 710 kJ mol⁻¹ for EST2 to 620 kJ mol⁻¹ for K102Q and 460 kJ mol⁻¹ for EST2-36del; the value of $\Delta_d C_{p,2} = 9$ kJ K⁻¹mol⁻¹ for all the three proteins.

If the two transitions correspond to the unfolding of two independent domains, the thermodynamic stability of the latter can be calculated by the Gibbs-Helmholtz equation, whose integration, in the assumption that $\Delta_d C_p$ is a constant quantity, leads to [20,25]:

$$\Delta_d G(T) = \Delta_d H(T_d) \cdot [1 - (T/T_d)] + \Delta_d C_p \cdot [T - T_d - T \cdot \ln(T/T_d)] \quad (8)$$

The parabola-like stability curve of domain-1 shows $T_{max} = 297$ K for EST2, 292 K for K102Q and 295 K for EST2-36del, while $\Delta_d G_1(298 \text{ K}) = 37$ kJ mol⁻¹ for both EST2 and K102Q, and 18 kJ

mol⁻¹ for EST2-36del. The parabola-like stability curve of domain-2 shows $T_{\max} = 288$ K for EST2, 296 K for K102Q and 312 K for EST2-36del, while $\Delta_d G_2(298 \text{ K}) = 71$ kJ mol⁻¹ for EST2, 56 kJ mol⁻¹ for K102Q, and 28 kJ mol⁻¹ for EST2-36del. As a consequence, the total denaturation Gibbs energy change at room temperature amounts to 108 kJ mol⁻¹ for EST2, 93 kJ mol⁻¹ for K102Q and 46 kJ mol⁻¹ for EST2-36del. These numbers unequivocally clarify the strong destabilization of the folded structure caused by deleting the first 35 residues of EST2. In addition, the T_{\max} estimates of the two domains in the three proteins fall in the range 285 ± 19 K determined by Rees and Robertson on the basis of a large collection of experimental data [26].

Several structure-energetics relationships have been proposed in order to calculate the unfolding thermodynamics of globular proteins from their 3D structure. On the basis of a large data set, Robertson and Murphy arrived at the following relationships in which the structural parameter is simply the number of residues constituting the protein [27]:

$$\Delta_d C_p(\text{in kJ K}^{-1}\text{mol}^{-1}) \cong 0.058 \cdot N_{\text{res}}, \text{ with } r = 0.86 \quad (9)$$

$$\Delta_d H(T = 333 \text{ K}; \text{ in kJ mol}^{-1}) \cong 2.92 \cdot N_{\text{res}}, \text{ with } r = 0.77 \quad (10)$$

Accordingly, for a protein of 310 residues such as EST2, $\Delta_d C_p$ should amount to 18 kJ K⁻¹mol⁻¹ and $\Delta_d H(T = 333 \text{ K})$ to 905 kJ mol⁻¹. Experimental data for EST2, $\Delta_d C_p = 16$ kJ K⁻¹mol⁻¹ and $\Delta_d H(T = 333 \text{ K}) = 870$ kJ mol⁻¹ are in line with the estimates from Eqs. (9) and (10), by recognizing that it is a thermophilic protein not well represented as a single cooperative domain.

The conformational stability of the three protein forms has been investigated also with respect to the denaturing action of urea and GuHCl, by performing CD and fluorescence measurements. It is worth noting that both the urea-induced unfolding and GuHCl-induced unfolding of the three proteins are reversible processes: a full recovery of all of the spectroscopic features of the native state is observed upon suitable dilution of completely unfolded samples. The transition curves obtained by recording the molar ellipticity at 222 nm, 20 °C and pH 7.5, 20 mM phosphate buffer, are shown in Figure 8. These transition curves have a sigmoidal shape, suggestive of a cooperative process, and approach zero demonstrating that there is no residual secondary

structure in the chemically unfolded proteins. In contrast, thermally unfolded protein samples show large negative values of molar ellipticity at 222 nm (see Figure 2a). Similar sigmoidal transition curves have been obtained by fluorescence measurements probing the tertiary structure (not shown). It is worth noting that, upon excitation at 280 nm: (a) EST2 and K102Q show a fluorescence emission spectrum with a maximum at 337 nm that shifts to 350 nm upon unfolding; (b) EST2-36del shows a fluorescence emission spectrum with a maximum at 339 nm that shifts to 351 nm upon unfolding (data not shown). The values of the denaturant concentration at the transition midpoint are listed in Table 3. In particular: $[\text{urea}]_{1/2} = 5.9 \text{ M}$ for EST2, 5.7 M for K102Q and 4.6 M for EST2-36del; $[\text{GuHCl}]_{1/2} = 1.9 \text{ M}$ for EST2, 2.2 M for both K102Q and EST2-36del. These numbers indicate that, while the stability against urea follows a scale similar to that found in the case of temperature, the stability against GuHCl of the two variant forms is larger than that of EST2. Such values, coupled with the cooperativity of the sigmoidal transition curves, confirm that chemical denaturants such as urea and GuHCl unfold globular proteins using a mechanism entirely different from that adopted by temperature [6,7,28].

4. Discussion

We would like to provide an interpretation of the present data by considering that the structure of EST2 consists of two interacting domains. The temperature-induced unfolding process of EST2, as previously reported [6,7], resembles a two-state $N \rightleftharpoons D$ transition, if investigated by means of far-UV CD measurements. In contrast, near-UV CD transition curves and DSC traces emphasize that the process is not a two-state $N \rightleftharpoons D$ transition. The coupling of the two domains weakens on performing both the K102Q point mutation and the deletion of the first 35 residues in the N-terminal region. The qualitatively similar effect caused by the point mutation and the N-terminal deletion merits attention. According to the X-ray structure of EST2, the side chains of K102 and E43 form a salt-bridge on the protein surface [9]. The nitrogen atom of the amino group in the K102 side chain is at 3.5 Å and 4.4 Å, respectively, from the two oxygen atoms of the carboxylate group in the E43 side chain. The mutation K102Q renders impossible the formation of the salt-bridge with the side chain of E43 and destroys a strong interaction between the N-terminal region and the core of EST2 structure. However, it is not correct to identify one of the two domains

simply with the so-called “cap” domain, recognized in the X-ray structure of EST2 and containing the protein N-terminal region [9].

In fact, the deletion of the first 35 residues of the polypeptide chain does not lead to a more cooperative thermal unfolding process, as could be expected. It seems to cause the loss of important interactions between the two domains that, as a consequence, behave in a much more independent manner with respect to the resistance against temperature. One can suggest that the external shell of EST2 structure corresponds to the less stable domain, while the core region of EST2 structure corresponds to the more stable domain. Both the point mutation K102Q and the deletion of the N-terminal region seem to cause the loss of critical interactions between the external shell and the core region of the protein. The presence of two domains in a protein consisting of 310 residues would be in line with both theoretical and experimental findings, suggesting that a single cooperative domain should have a maximum size of about 200 residues [29-31]. However, structural features of the α/β hydrolase fold of EST2, with nine α -helices packed against the central twisted β -sheet, do not allow an unambiguous identification of the two coupled domains.

Experimental measurements and deconvolution analyses indicate that one of the two domains is more stable with a denaturation temperature of 86 °C, common to all the three proteins, whereas the other domain has a denaturation temperature that decreases from 81 °C for EST2 to 76 °C for K102Q and 62 °C for EST2-36del. The T_d value of the more stable domain is absolutely not affected by the point mutation or by the N-terminal deletion, even though the corresponding enthalpy changes are smaller. In general, the denaturation temperature $T_d = \Delta_d H / \Delta_d S$ [20,21], where $\Delta_d S$ is the entropy change associated with the denaturation process. Since $T_{d,2}$ is 86 °C for both EST2 and EST2-36del, even though $\Delta_d H_2 = 710 \text{ kJ mol}^{-1}$ for the former and 460 kJ mol^{-1} for the latter, the $\Delta_d S_2$ value of the truncated form is expected to be significantly smaller than that of wild-type. Because the thermally denatured states of all the three proteins are closely similar, as indicated by far-UV and near-UV CD spectra (see Figure 2), this difference in entropy should be a manifestation of a greater conformational flexibility of the more stable domain in the folded state of EST2-36del. The deletion of the N-terminal region seems to lead to a less rigid core domain. A qualitatively similar situation occurs for K102Q.

In contrast, the weakening of the coupling causes a marked decrease in the denaturation temperature of the external domain exactly because it needs to interact with the core domain to enhance its own thermal resistance. The loss of the important salt-bridge between E43 and K102 side chains upon the K102Q mutation destabilizes this domain, even though the $\Delta_d H_1$ value is 440 kJ mol⁻¹ as for EST2. The deletion of the first 35 residues in the N-terminal region strongly destabilizes this external domain, leading to a decrease of $T_{d,1}$ from 81 to 62 °C.

Following the original approaches developed by Brandts and co-workers [32], and Freire and co-workers [33], we have devised a model of two cooperative and coupled domains able to reproduce the main qualitative features of the DSC curves shown by the three investigated proteins. The partition function for a globular protein consisting of two cooperative and coupled domains can be written by considering that: (a) domain-1 is less stable than domain-2 with respect to temperature (i.e., $T_{d,1} < T_{d,2}$); (b) coupling interactions are operative solely when both domains are folded (i.e., unfolding of domain-1 disrupts coupling interactions at the interface between the two domains); (c) as a consequence, the coupling parameter $\phi_{12} = \exp(-\Delta G_{12}/RT)$, where ΔG_{12} is the coupling Gibbs energy change, is operative during the unfolding of domain-1 and then becomes equal to 1 (i.e., $\phi_{12} = 1$ means $\Delta G_{12} = 0$, no coupling occurs); (d) the coupling Gibbs energy change is purely entropic, $\Delta G_{12} = -T \cdot \Delta S_{12}$, so that $\phi_{12} = \exp(-T \cdot \Delta S_{12}/RT) = \exp(-\Delta S_{12}/R)$ proves to be a temperature independent quantity, and does not provide an enthalpy contribution to the unfolding process. The corresponding canonical partition function, by assuming the native state as reference, is:

$$Q_{\text{coupling}}(T) = (1 + \phi_{12} \cdot K_1) \cdot (1 + K_2) \quad (11)$$

and the excess enthalpy function, by considering $\Delta_d C_{p,1} = \Delta_d C_{p,2} = 0$ for simplicity, can be written as:

$$\langle \Delta H(T) \rangle_{\text{coupling}} = \Delta_d H_1 \cdot [\phi_{12} \cdot K_1 / (1 + \phi_{12} \cdot K_1)] + \Delta_d H_2 \cdot [K_2 / (1 + K_2)] \quad (12)$$

Actually, the latter is an approximate expression of the excess enthalpy function for two “practically independent” domains in the assumption that the stability of domain-1 is affected by coupling

interactions and that of domain-2 is not affected. By performing the temperature derivative of Eq. (12), one obtains the excess heat capacity function for this model. On the basis of a bunch of calculations, we have determined a single set of thermodynamic parameters that produce the simulated DSC curves shown in Figure 9, that qualitatively reproduce the experimental ones reported in Figure 7. The parameter values are: $T_{d,1} = 335.2$ K, $\Delta_d H_1 = 400$ kJ mol⁻¹, $T_{d,2} = 359.2$ K, $\Delta_d H_2 = 600$ kJ mol⁻¹ and $\phi_{12} = 1$ (curve *a*), $\phi_{12} = 0.003$ (curve *b*), $\phi_{12} = 0.0008$ (curve *c*). The two denaturation temperatures are the ones experimentally found for EST2-36del in the assumption that in this protein the two domains are not coupled (note that the values of $\Delta_d H_1$ and $\Delta_d H_2$ do not affect the temperature location of the simulated DSC peaks). When the coupling parameter $\phi_{12} < 1$, the first unfolding transition occurs at higher temperature: (a) 349.2 K for $\phi_{12} = 0.003$, as in the case of K102Q; (b) 354.2 K for $\phi_{12} = 0.0008$, as in the case of EST2. In other words, the occurrence of coupling interactions stabilizes the less stable of the two domains. These coupling interactions, according to the present model calculations, amount to: (a) $\Delta G_{12} = 16.2$ kJ mol⁻¹ at 335.2 K for K102Q (i.e., $\Delta S_{12} = -48.3$ J K⁻¹mol⁻¹); (b) $\Delta G_{12} = 19.9$ kJ mol⁻¹ at 335.2 K for EST2 (i.e., $\Delta S_{12} = -59.4$ J K⁻¹mol⁻¹). The assumption that ΔG_{12} is purely entropic is not absurd; it may correspond to the dominance of the hydrophobic effect in the interactions that couple the two domains (i.e., it is widely accepted that the hydrophobic effect is entropic in nature [34]). The ability of a model to reproduce some features of experimental data does not necessarily imply the rightness of the model. Our aim is to underscore that the occurrence of coupling interactions between two cooperative domains can explain the experimental data for EST2 and the two mutant forms. In order to identify cooperative domains in globular proteins it is tacitly assumed the structural invariance of the native state on increasing temperature. Since this assumption could not be strictly accurate, it should be useful to perform molecular dynamics simulations at different temperatures to test the behaviour of the folded conformations. Molecular dynamics simulations at different temperatures are in progress on both EST2 and the deleted variant in order to try to discover the two domains and the origin of the marked destabilization of one of them due to deletion.

In conclusion, the present data indicate that the thermal unfolding of EST2 and the two variant forms K102Q and EST2-36del is a reversible process not well represented as a two-state

$N \rightleftharpoons D$ transition. It emerges the presence of two coupled domains in the EST2 structure, even though further measurements on other mutant forms would be necessary to unambiguously define such two domains in the native structure of EST2. Moreover, experimental data indicate that the conformational stability of the three proteins against temperature does not parallel that against urea and GuHCl. This finding suggests that strategies to increase protein stability against temperature should be different from those able to enhance protein stability against chemical denaturants.

Acknowledgements. Work supported by grants from the Italian Ministry for Education, University and Research (MIUR, Roma), and Centro Regionale di Competenza per l'Analisi e il Monitoraggio Ambientale (AMRA, Napoli). The technical support of Centro Interdipartimentale di Metodologie Chimico-Fisiche (CIMCF, Università di Napoli Federico II) is gratefully acknowledged.

References

1. G. Manco, E. Adinolfi, F.M. Pisani, V. Carratore, M. Rossi, Identification of an esterase from *Bacillus acidocaldarius* with sequence similarity to a hormone sensitive lipase subfamily, *Prot. Pept. Lett.* 4 (1997) 375-382.
2. G. Manco, E. Adinolfi, F.M. Pisani, G. Ottolina, G. Carrea, G. Manco, Overexpression and properties of a new thermophilic and thermostable esterase from *Bacillus acidocaldarius* with sequence similarity to hormone-sensitive lipase subfamily, *Biochem. J.* 332 (1998) 203-212.
3. H. Hemilä, T.T. Koivula, I. Palva, Hormone-sensitive lipase is closely related to several bacterial proteins and distantly related to acetylcholinesterase and lipoprotein lipase: identification of a superfamily of esterases and lipases, *Biochim. Biophys. Acta* 1210 (1994) 249-253.
4. G. Manco, F. Febbraio, E. Adinolfi, M. Rossi, Homology modeling and active-site residues probing of the thermophilic *Alicyclobacillus acidocaldarius* esterase 2, *Protein Sci.* 8 (1999) 1789-1796.
5. G. Manco, L. Mandrich, M. Rossi, Residues at the active site of the esterase 2 from *Alicyclobacillus acidocaldarius* involved in substrate specificity and catalytic activity at high temperature, *J. Biol. Chem.* 276 (2001) 37482-37490.
6. P. Del Vecchio, G. Graziano, V. Granata, G. Barone, L. Mandrich, G. Manco, M. Rossi, Temperature- and denaturant-induced unfolding of two thermophilic esterases, *Biochemistry* 41 (2002) 1364-1371.
7. P. Del Vecchio, G. Graziano, V. Granata, G. Barone, L. Mandrich, G. Manco, M. Rossi, Denaturing action of urea and guanidine hydrochloride towards two thermophilic esterases, *Biochem. J.* 367 (2002) 857-863.
8. L. Mandrich, M. Pezzullo, P. Del Vecchio, G. Barone, M. Rossi, G. Manco, Analysis of thermal adaptation in the HSL enzyme family, *J. Mol. Biol.* 335 (2004) 357-369.
9. G. De Simone, S. Galdiero, G. Manco, D. Lang, M. Rossi, C. Pedone, A snapshot of a transition state analogue of a novel thermophilic esterase belonging to the subfamily of mammalian hormone-sensitive lipase, *J. Mol. Biol.* 303 (2000) 761-771.

10. G. De Simone, L. Mandrich, V. Menchise, V. Giordano, F. Febbraio, M. Rossi, C. Pedone, G. Manco, A substrate-induced switch in the reaction mechanism of thermophilic esterase, *J. Biol. Chem.* 279 (2004) 6815-6823.
11. L. Mandrich, L. Merone, M. Pezzullo, L. Cipolla, F. Nicotra, M. Rossi, G. Manco, Role of the N-terminus in enzyme activity, stability and specificity in thermophilic esterases belonging to the HSL family, *J. Mol. Biol.* 345 (2005) 501-512.
12. S.C. Gill, P.H. von Hippel, Calculation of protein extinction coefficients from amino acid sequence data, *Anal. Biochem.* 182 (1989) 319-326.
13. C.N. Pace, Determination and analysis of urea and guanidine hydrochloride denaturation curves, *Methods Enzymol.* 131 (1986) 266-280.
14. S.Y. Venyaminov, J.T. Yang, Determination of protein secondary structure, in: G.D. Fasman (Ed.), *Circular Dichroism and the Conformational Analysis of Biomolecules*, Plenum Press, New York, 1996, pp. 69-107.
15. N. Sreema, R.W. Woody, A self-consistent method for the analysis of protein secondary structure from circular dichroism, *Anal. Biochem.* 209 (1993) 32-44.
16. A. Lobley, A.L. Whitmore, B.A. Wallace, Dichroweb: an interactive website for the analysis of secondary structure from circular dichroism data, *Bioinformatics* 18 (2002) 211-212.
17. J.R. Lakowicz, *Principles of Fluorescence Spectroscopy*, Kluwer Academic and Plenum Publishers, New York, 1999.
18. F. Catanzano, C. Giancola, G. Graziano, G. Barone, Temperature-induced denaturation of ribonuclease S: a thermodynamic study, *Biochemistry* 35 (1996) 13378-13385.
19. E. Freire, R.L. Biltonen, Statistical mechanical deconvolution of thermal transitions in macromolecules I. Theory and application to homogeneous systems, *Biopolymers* 17 (1978) 463-479.
20. P.L. Privalov, Stability of proteins: small globular proteins, *Adv. Protein Chem.* 33 (1979) 167-241.
21. Y. Zhou, C.K. Hall, M. Karplus, The calorimetric criterion for a two-state process revisited, *Protein Sci.* 5 (1999) 1064-1074.

22. F. Catanzano, A. Gambuti, G. Graziano, G. Barone, Interaction with D-glucose and thermal denaturation of yeast hexokinase B: a DSC study, *J. Biochem.* 121 (1997) 568-577.
23. E. Freire, Statistical thermodynamic analysis of differential scanning calorimetry data: structural deconvolution of heat capacity function of proteins, *Methods Enzymol.* 240 (1994) 502-530.
24. S. J. Gill, B. Richey, G. Bishop, J. Wyman, Generalized binding phenomena in an allosteric macromolecule, *Biophys. Chem.* 21 (1985) 1-14.
25. W. J. Becktel, J. A. Schellman, Protein stability curves, *Biopolymers* 26 (1987) 1859-1877.
26. D. C. Rees, A. D. Robertson, Some thermodynamic implications for the thermostability of proteins, *Protein Sci.* 10 (2001) 1187-1194.
27. A. D. Robertson, K. P. Murphy, Protein structure and energetics of protein stability, *Chem. Rev.* 97 (1997) 1251-1267.
28. R. Jaenicke, G. Bohm, The stability of proteins in extreme environments, *Curr. Opin. Struct. Biol.* 8 (1998) 738-748.
29. K. A. Dill, Theory for the folding and stability of globular proteins, *Biochemistry* 24 (1985) 1501-1509.
30. P. L. Privalov, Thermodynamic problems of protein structure, *Annu. Rev. Biophys. Biophys. Chem.* 18 (1989) 47-69.
31. V. Z. Spassov, A. D. Karshikoff, R. Ladenstein, The optimisation of protein-solvent interactions: thermostability and the role of hydrophobic and electrostatic interactions, *Protein Sci.* 4 (1995) 1516-1527.
32. J. F. Brandts, C. Q. Hu, L. N. Lin, A simple model for proteins with interacting domains. Applications to scanning calorimetry data, *Biochemistry* 28 (1989) 8588-8596.
33. G. Ramsay, E. Freire, Linked thermal and solute perturbation analysis of cooperative domain interactions in proteins. Structural stability of diphtheria toxin, *Biochemistry* 29 (1990) 8677-8683.
34. G. Graziano, Scaled particle theory study of the lengthscale dependence of cavity thermodynamics in different liquids, *J.Phys.Chem.B* 110 (2006) 11421-11426.

Table 1. Thermodynamic data for the thermal unfolding at pH 7.5, 20 mM phosphate buffer of EST2, K102Q and EST2-36del, investigated by means of DSC and CD measurements, using always a scanning rate of 1.0 K min⁻¹.

	probe	T _d °C	Δ _d H(cal) kJ mol ⁻¹	Δ _d H(vH) kJ mol ⁻¹	Δ _d C _p kJ K ⁻¹ mol ⁻¹
EST2	DSC	86	1110	530	16
	CD(222 nm)	91		440	
	CD(290 nm)	86		510	
K102Q	DSC	86	1020	430	16
	CD(222 nm)	86		340	
	CD(290 nm)	86		360	
EST2-36del	DSC	86	750	350	16
	CD(222 nm)	86		260	
	CD(290 nm)	86		640	

Note. Each value is the average over four measurements; the error in T_d does not exceed 0.2 °C. The estimated relative uncertainties in Δ_dH and Δ_dC_p amount to 5% and 10%, respectively, of reported values.

Table 2. Values of the thermodynamic parameters obtained from the deconvolution analysis of DSC curves by means of the independent model (first line of each protein) and the sequential model (second line of each protein).

	$T_{d,1}$ °C	$\Delta_d H_1$ kJ mol ⁻¹	$\Delta_d C_{p,1}$ kJ K ⁻¹ mol ⁻¹	$T_{d,2}$ °C	$\Delta_d H_2$ kJ mol ⁻¹	$\Delta_d C_{p,2}$ kJ K ⁻¹ mol ⁻¹
EST2	81	440	7	86	710	9
	81	440	7	86	690	9
K102Q	76	440	7	86	620	9
	76	420	7	86	590	9
EST2-36del	62	300	7	86	460	9
	62	300	7	86	460	9

Note. The reported numbers are the average values obtained by performing the nonlinear regression over four independent DSC curves, according to the independent model and the sequential one, respectively. The errors in $T_{d,i}$ do not exceed 0.4 °C, while the relative uncertainties in $\Delta_d H_i$ and $\Delta_d C_{p,i}$ amount to 5% of the reported values.

Table 3. Values of the urea and GuHCl concentrations at the midpoint of the unfolding transition for EST2, K102Q and EST2-36del, determined by recording the molar ellipticity at 222 nm, the fluorescence intensity at 337 nm, and the shift in the maximum of fluorescence emission spectra at 20 °C, pH 7.5, 20 mM phosphate buffer.

	probe	[urea] _{1/2} M	[GuHCl] _{1/2} M
EST2	[θ] _{222 nm}	5.9	1.9
	I _{337 nm}	5.9	1.9
	λ_{\max}	5.8	2.0
K102Q	[θ] _{222 nm}	5.7	2.2
	I _{337 nm}	5.4	2.2
	λ_{\max}	5.7	2.4
EST2-36del	[θ] _{222 nm}	4.6	2.2
	I _{337 nm}	4.4	2.0
	λ_{\max}	4.6	2.2

Note. Each value is the average over four independent measurements, and the estimated relative uncertainties amount to 5% of reported values.

Captions to the Figures

Figure 1a. X-ray structure of EST2 (PDB code 1EVQ) from *Alicyclobacillus acidocaldarius*. The position of L36 is indicated and the side chains of E43 and K102, forming a salt-bridge on protein surface, are shown.

Figure 1b. Schematic representation of the secondary structure elements of EST2, showing in blue the “cap” domain. The position of the catalytic triad residues is shown together with that of L36 up to which the polypeptide chain of EST2 has been deleted, E43 and K102.

Figure 2a. Far-UV CD spectra of EST2 (circles), K102Q (squares) and EST2-36del (diamonds) recorded in 20 mM phosphate buffer at 20 °C (open symbols) and 108 °C (filled symbols). High temperature spectra of the three proteins are practically identical, while small differences are visible in room temperature spectra.

Figure 2b. Near-UV CD spectra of EST2 (circles), K102Q (squares) and EST2-36del (diamonds) recorded in 20 mM phosphate buffer at 20 °C (open symbols) and 108 °C (filled symbols). Loss of the positive band centred at 270 nm in the room temperature spectrum of EST2-36del is due to the loss of Y22. High temperature spectra of the three proteins are virtually identical.

Figure 3. Thermal unfolding curves of EST2 at pH 7.5, 20 mM phosphate buffer, obtained by recording the molar ellipticity at 222 nm (filled circles) and 290 nm (open squares). The two curves are different between each other, suggesting that the process is not a two-state transition.

Figure 4. Thermal unfolding curves of K102Q at pH 7.5, 20 mM phosphate buffer, obtained by recording the molar ellipticity at 222 nm (filled circles) and 290 nm (open squares). The two curves are different between each other, suggesting that the process is not a two-state transition.

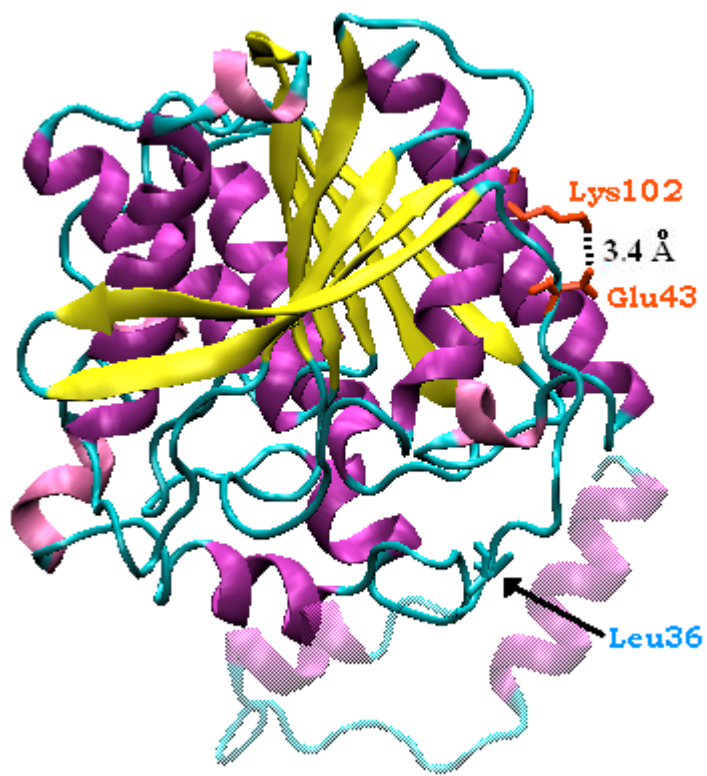
Figure 5. Thermal unfolding curves of EST2-36del at pH 7.5, 20 mM phosphate buffer, obtained by recording the molar ellipticity at 222 nm (filled circles) and 290 nm (open squares). The two curves are markedly different between each other, indicating that the process is not a two-state transition.

Figure 6. Reversibility of the thermal unfolding process of K102Q – first heating, open squares; second heating, filled squares – and EST2-36del – first heating, open diamonds; second heating, filled diamonds.

Figure 7. DSC traces recorded at pH 7.5, 20 mM phosphate buffer, for EST2 (bottom panel), K102Q (middle panel) and EST2-36 del (upper panel). The single peaks obtained by means of the deconvolution procedure, according to the independent model, and their sum are also shown for the three proteins (see text for further details).

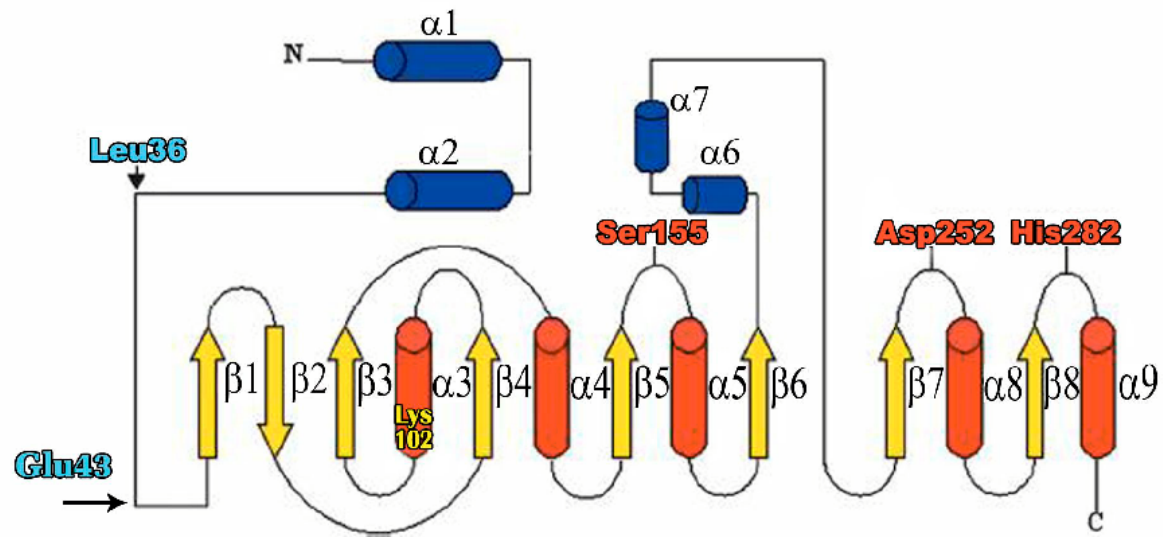
Figure 8. Denaturant-induced unfolding curves at 20 °C, pH 7.5, 20 mM phosphate buffer, for EST2 (circles), K102Q (squares) and EST2-36del (diamonds), obtained by recording the molar ellipticity at 222 nm. The urea-induced curves are centred around 5 M, while the GuHCl-induced curves are centred around 2 M. The points are connected by lines solely to guide the eyes.

Figure 9. Simulated DSC curves calculated on the basis of the model of Eqs. (11) and (12), qualitatively resembling the experimental ones shown in Figure 7. The parameter values used in the calculations are: $T_{d,1} = 335.2$ K, $\Delta_d H_1 = 400$ kJ mol⁻¹, $T_{d,2} = 359.2$ K, $\Delta_d H_2 = 600$ kJ mol⁻¹ and $\varphi_{12} = 1$ (curve *a*), $\varphi_{12} = 0.003$ (curve *b*), and $\varphi_{12} = 0.0008$ (curve *c*). See text for further details.

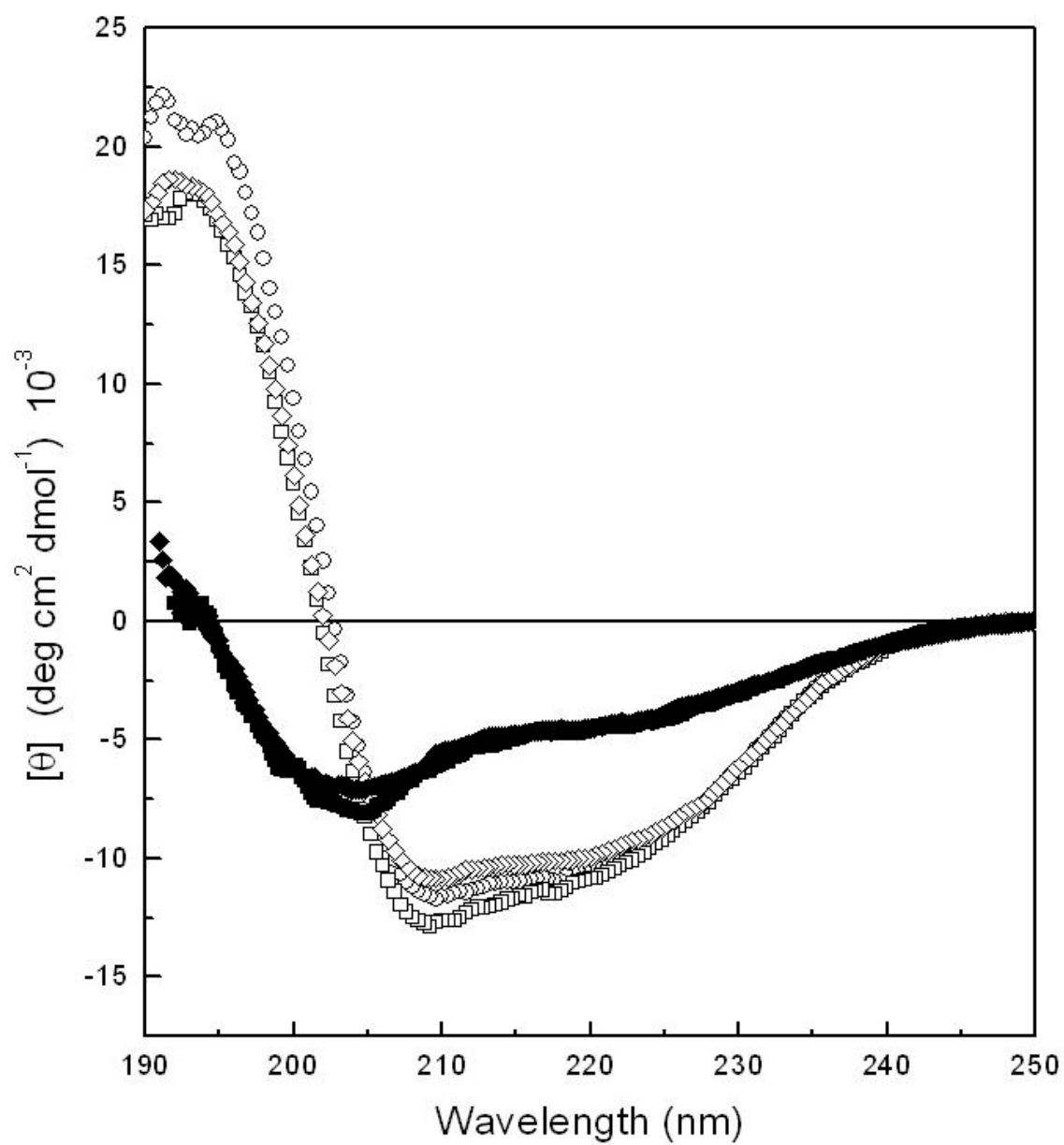


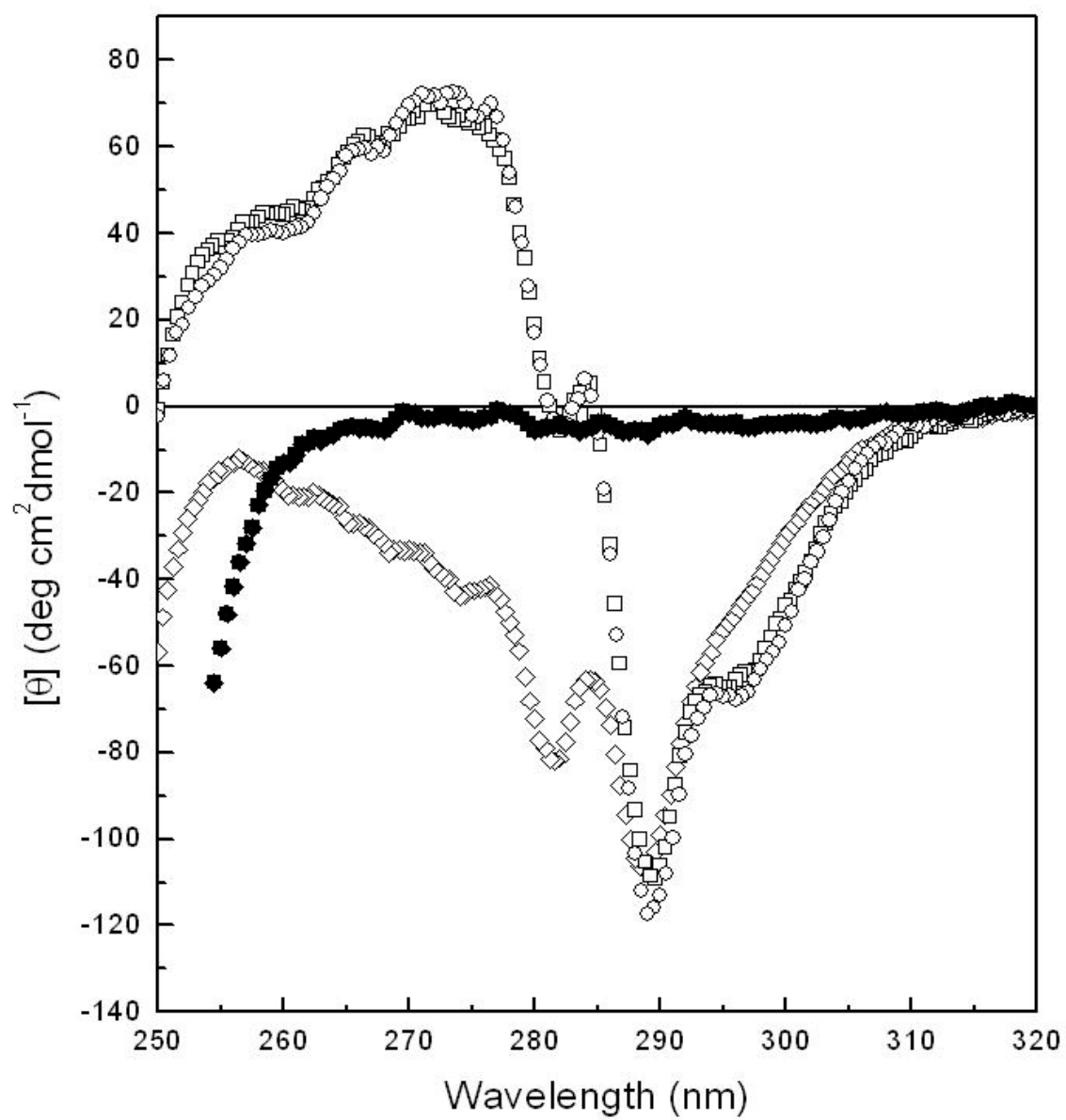
ACCEPTED

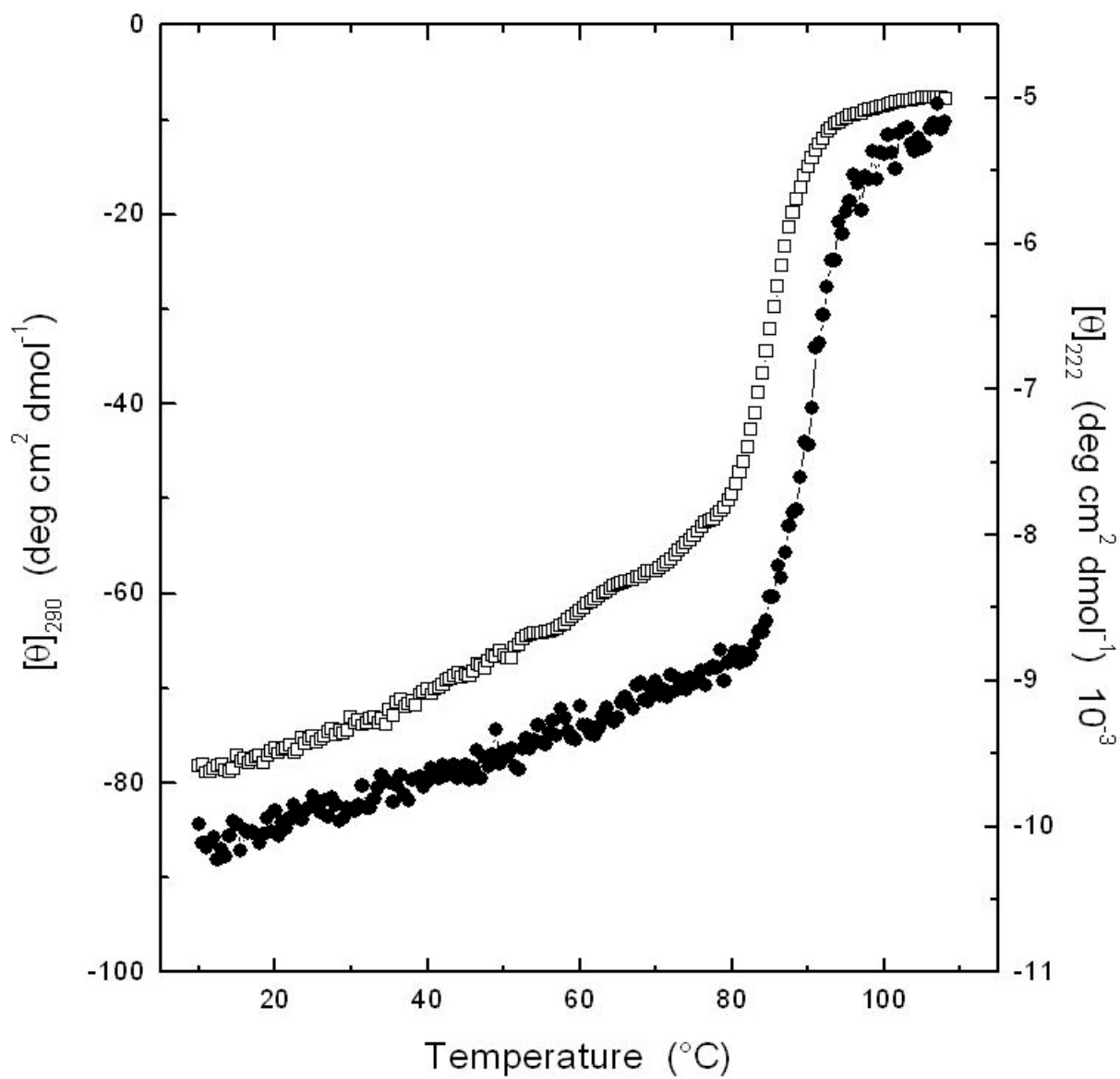
SCRIPT

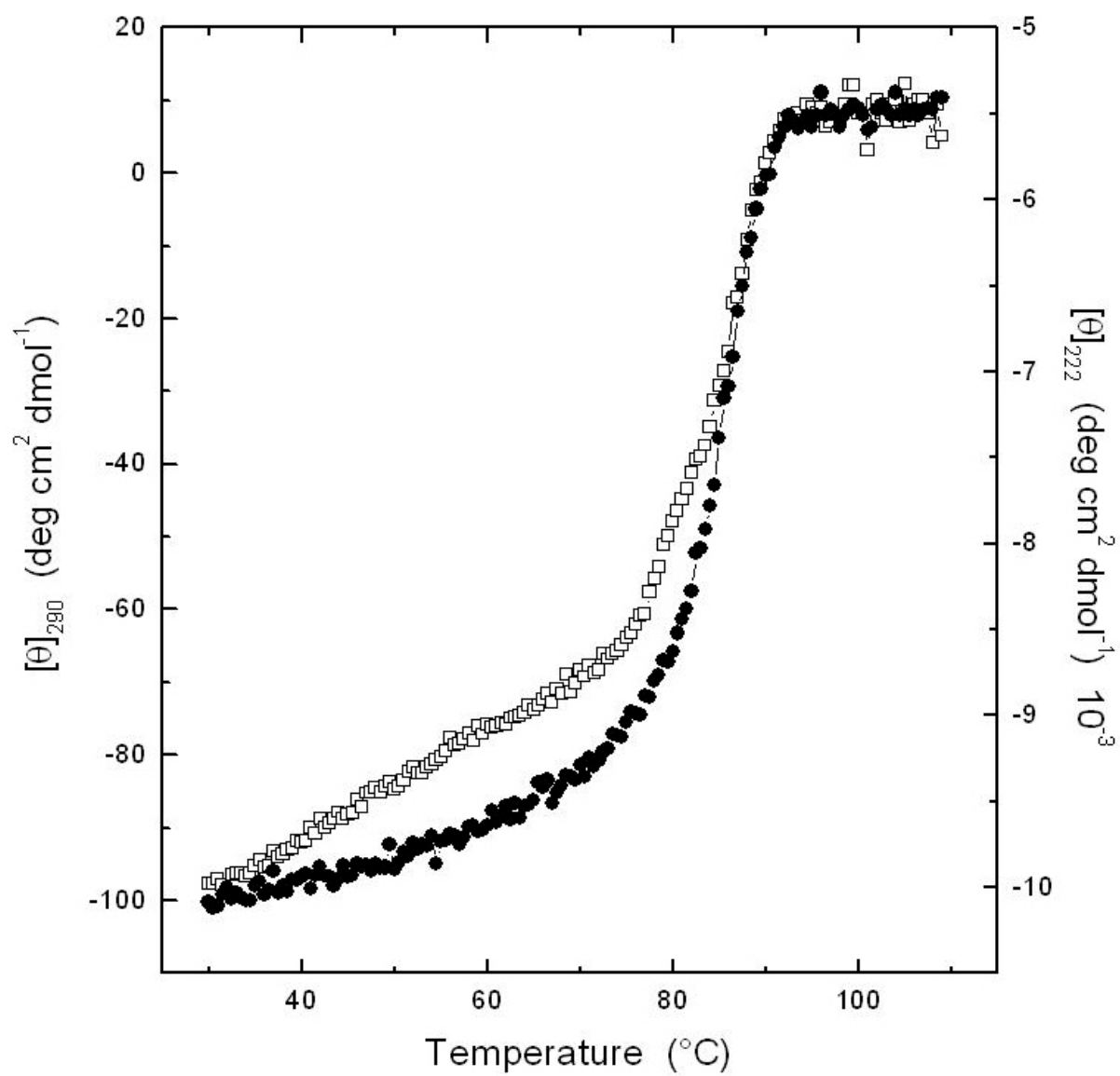


ACCEPTED MANUSCRIPT









A

